THE ASTROPHYSICAL JOURNAL, 560:261–271, 2001 October 10

THEORETICAL MODELING OF INFRARED EMISSION FROM NEUTRAL AND CHARGED POLYCYCLIC AROMATIC HYDROCARBONS. II.

E. L. O. BAKES
SETI Institute, NASA Ames Research Center, MS 245-3, Moffett Field, CA 94035
A. G. G. M. TIELENS
SRON, Kapteyn Astronomical Institute, P.O. Box 800, 9700 AV Groningen, The Netherlands
CHARLES W. BAUSCHLICHER, JR.
NASA Ames Research Center, MS 230-3, Moffett Field, CA 94035
AND
DOUGLAS M. HUDGINS AND LOUIS J. ALLAMANDOLA
NASA Ames Research Center, MS 245-6, Moffett Field, CA 94035
Received 2001 April 2; accepted 2001 June 18

ABSTRACT

The nature of the carriers of the interstellar infrared (IR) emission features between 3.3 and 12.7 μm is complex. We must consider emission from a family of polycyclic aromatic hydrocarbons (PAHs) in a multiplicity of cationic charge states (+1, +2, +3, and so on), along with neutral and anionic PAHs. The adopted intrinsic IR cross sections of the various modes of the PAHs are the key to all models. Here we make a comparison between laboratory-measured cross sections and quantum chemical calculations and find that, overall, the agreement is very good. In this paper, we consider emission from a wide variety of specific PAH molecules, which includes all available data from our laboratory and quantum chemical databases. We incorporate this into our model to produce a theoretical analysis that is more realistic, detailed, and comprehensive than prior studies. PAH molecular structures that we consider include symmetric condensed, symmetric noncondensed, aromatics containing pentagonal rings, linear, and methylated PAHs. The synthesized IR spectra show large variations in peak position for the small PAHs studied, while their spectral profile is uniquely characteristic of each different molecular structure. We also investigate the spectral variations with molecular structure of a PAH population at the surface of the Orion photodissociation region (PDR) and include an example of how the IR spectrum of our PAH population varies dramatically as a function of depth (or radiation field) through the PDR. We make a comparison of these results with *Infrared Space Observatory* data measured at the surface of the Orion PDR. We conclude that the charge of PAHs in a composite population has a stronger effect on its IR emission spectrum than its molecular structure. However, on the basis of the PAH samples considered in this paper, detailed studies of the interstellar IR emission features can be used effectively to identify molecular characteristics of the interstellar PAH family. In Paper III, we extend the theme of this paper by investigating the effects of hydrogenation on a wide variety of PAHs up to size 54 carbon atoms and compare our results with observational profiles for the Orion PDR.

Subject headings: ISM: lines and bands — ISM: molecules — infrared: ISM — methods: analytical — molecular processes

1. INTRODUCTION

Strong infrared (IR) emission features at 3.3, 6.2, 7.7, 8.6, 11.2, and 12.7 μm are observed in many astronomical sources. Recent *Infrared Space Observatory* (*ISO*) observations have shown that these ubiquitous IR emission features are the most luminous spectral features from the interstellar medium (ISM) in our own and other galaxies. These features have been assigned to polycyclic aromatic hydrocarbon molecules (PAHs; Léger & Puget 1984; Allamandola, Tielens, & Barker 1985, hereafter ATB85; Allamandola, Tielens, & Barker 1989, hereafter ATB89; Puget & Léger 1989), although the exact molecular identification of the carriers of these IR features has remained elusive. When a PAH absorbs an interstellar ultraviolet (UV) photon, a vibrationally excited molecule is produced, which relaxes by IR emission. In this way, PAHs are the dominant contributors to the mid-IR spectrum of many interstellar regions, including photodissociation regions (PDRs) associated with regions of massive star formation, dust enshrouded stellar objects, and galactic nuclei. PAHs mediate the interstellar energy balance in these objects by controlling the conversion of UV to IR radiation.

This paper is part of a series of papers that model the IR emission from a family of interstellar PAHs. The model is based upon an extensive database of intrinsic IR cross sections of PAHs, either measured in the laboratory using matrix isolation spectroscopy or calculated quantum mechanically. In Paper I (Bakes, Tielens, & Bauschlicher 2001, hereafter BTB2001), we have investigated the role of charge in the emerging IR spectra of interstellar PAHs. In that study, we concentrated on a set of six compact, condensed, symmetric PAHs with sizes ranging from 16 to 54 carbon atoms and demonstrated that charge is a key factor in determining the profile of individual features in the interstellar IR emission spectra. Here we extend that study by including all PAHs for which data on the intrinsic strength of their IR vibrational modes are available. The goal of this paper is to determine the effects of the molecular structure of PAHs on the resulting IR emission spectra. By doing this, we are able to more fully address the fundamental question

of the existence and characteristics of the family of PAHs in the ISM. This is made possible by the unique, comprehensive PAH spectral database made available by both the Quantum Chemistry Group and the Astrochemistry Laboratory at NASA Ames Research Center. Because each PAH has its own unique IR spectral signature when looked at in detail, which "fingerprints" both its molecular structure and its electrical charge, we may be able to identify specific classes of PAHs that contribute to IR emission from different interstellar regions. The sets of PAH molecules considered in this paper consist of symmetric condensed PAHs, symmetric noncondensed PAHs, aromatics with one pentagonal ring, methylated PAHs, and PAHs with a linear geometry and are listed in Table 1, where "L" indicates that the IR spectral properties of these PAH species are available in the laboratory database and "T" indicates that the IR spectral properties of these PAH species are available in the quantum chemical database. By combining these spectra according to their relative weights in our model, we are able to synthesize the resulting composite PAH emission spectra as a function of depth through the Orion PDR and compare this to the emerging IR emission.

In summary, the model described in this paper has been formulated to provide a theoretical basis on which direct quantitative interpretation of spectral IR emission data can be made. The emphasis is on the IR emission characteristics of the surface layer of the Orion bar and the interpretation and the analysis of and comparison with observational IR data between 3.3 and 12.7 μm. In § 2, we discuss the model and the IR spectral characteristics of each PAH family. In § 3, we explore the effects of PAH molecular structure on the interstellar IR emission spectrum and quantify the probable variation in profile with varying UV field and electron density. In § 4, we discuss the implications of our results for the Orion PDR and compare them with observational data from *ISO*, and finally, in § 5, we summarize our conclusions. In Paper III, we extend the theme of this paper by investigating the effects of hydrogenation on a wide variety of PAHs up to 54 carbon atoms in size. The chemistry of PAHH+ is complex and requires a thorough and detailed analysis, because hydrogenation is strongly affected by the charge of the PAH and the position at which a hydrogen atom is added onto the PAH. We will also make a preliminary comparison of our model results with observational data for the Orion PDR to ascertain the effects of hydrogenation and dehydrogenation on the interstellar IR emission features through the PDR.

2. MODELING THE IR SPECTRA OF THE INTERSTELLAR PAH FAMILY

2.1. *The Model*

When interstellar PAHs absorb a UV photon, the electronic energy is quickly transferred to the vibrational manifold, leaving the species vibrationally excited. Experimental work by Chercheneff & Barker (1989), Brenner & Barker

TABLE 1

AVAILABLE SPECTRA FOR BROAD PAH CLASSES

Molecule	Formula	Anion	Neutral	+1	+2	+3
Symmetric Condensed						
Pyrene	$C_{16}H_{10}$	...	LT	LT	...	...
Coronene	$C_{24}H_{12}$	...	LT	LT	T	...
Ovalene	$C_{32}H_{14}$	T	LT	LT	T	...
Hexabenzocoronene	$C_{42}H_{18}$	T	LT	LT	T	...
Dicoronylene	$C_{48}H_{20}$	T	LT	LT	T	T
Circumcoronene	$C_{54}H_{18}$	T	LT	LT	T	T
Symmetric Noncondensed						
Phenanthrene	$C_{14}H_{10}$	...	LT	LT	...	...
Triphenylene	$C_{18}H_{12}$	T	LT	LT	...	...
Benzophenanthrene	$C_{18}H_{12}$	...	LT	LT	...	...
Chrysene	$C_{18}H_{12}$	...	LT	LT	...	...
Perylene	$C_{20}H_{12}$	...	LT	LT	T	...
Linear						
Naphthalene	$C_{10}H_{8}$	T	LT	LT	...	...
Anthracene	$C_{14}H_{10}$	...	LT	LT	...	...
Tetracene	$C_{18}H_{12}$	T	LT	LT	...	...
Pentacene	$C_{22}H_{14}$	T	LT	LT	T	...
Pentagonal Rings						
Acenaphthylene	$C_{12}H_{8}$	...	LT	T	...	...
Fluoroanthene	$C_{16}H_{10}$	...	LT	LT	...	...
Benzo(a)fluoranthrene	$C_{20}H_{12}$	T	LT	LT	...	...
benzo(b)fluoranthrene	$C_{20}H_{12}$	...	LT	LT	...	...
Benzo(j)fluoranthrene	$C_{20}H_{12}$	T	LT	LT	...	...
Benzo(k)fluoranthrene	$C_{20}H_{12}$	...	LT	LT	...	...
Methyl Groups						
1- and 2-methylnaphthalene	$C_{11}H_{11}$	...	LT	LT	...	...
1-, 2-, and 9-methylanthracene	$C_{15}H_{13}$	...	LT	LT	...	...

(1992) and Saykally and colleagues (Cook & Saykally 1998) have confirmed that IR fluorescence from such molecular-sized species is well described by the RRKM quantum excitation proposed by ATB85 and approximated by the absorption cross section convolved with the Planck function, as first proposed by Léger & Puget (1984). This approach has formed the foundations of almost all theoretical modeling studies of interstellar PAH emission from the beginning (Léger & Puget 1984; ATB85; ATB89; Puget & Lèger 1989; Désert, Boulanger, & Puget 1990; Schutte, Tielens, & Allamandola 1993).

Previous models of IR emission from PAHs and carbonaceous grains (Draine & Anderson 1985; Désert et al. 1990; Schutte et al. 1993) modeled the IR emission from the ISM, taking the limited heat capacity of small grains and molecules into account. In particular, the model of Schutte et al. (1993) considered a size distribution of neutral PAHs and concluded that PAHs composed of less than 100 carbon atoms dominate the 3.3 μm emission, while larger PAHs contribute to the longer wavelength emission. However, in view of the lack of a comprehensive IR spectral database of specific PAH molecules, Schutte et al. (1993) had to use a trial and error method to determine "generic" PAH IR characteristics consistent with the observed IR emission spectrum of the Orion bar. In recent years, a large experimental and theoretical data set on neutral and ionized PAH IR cross sections has become available (Langhoff 1996; Bauschlicher & Langhoff 1997; Hudgins, Bauschlicher, & Allamandola 2001). Piest, von Helden, & Meijer (1999) followed these matrix isolation studies and quantum chemical calculations with experimental measurements of the absorption spectrum cross sections for gas phase cationic naphthalene, confirming that the matrix isolation and theoretical spectra were indeed applicable to the IR emission studies. It is therefore timely to revisit models for the IR emission of interstellar PAHs using realistic PAH properties.

We combine the PAH and carbonaceous dust grain charge distribution (Bakes & Tielens 1994, hereafter BT94) with the work of Bakes (1992) and Schutte et al. (1993) on the temperature distribution of UV pumped interstellar PAHs. Our model calculates the expected IR spectrum of any size of interstellar PAH or small grain of any charge state as a function of the UV field in an interstellar region. The adopted UV absorption properties are based on BT94, tailored to the specific PAH and UV field considered. The adopted PAH IR emission properties are based on the most recent laboratory data and quantum chemical studies of PAH species (Bauschlicher & Bakes 2000; Hudgins & Allamandola 1999a, 1999b and references therein; Langhoff 1996). Together with the calculated charge distribution function, the IR emission spectrum of any PAH can then be evaluated. This model yields detailed information on the IR spectra of a family of PAHs and its dependence on the size, molecular structure, charge state, and evolution of the emitters in a broad variety of interstellar conditions.

To correctly synthesize PAH IR emission, it is essential to consider the IR emission intensity from each PAH in the interstellar population in each of its probable charge states. The total line intensity I_i owing to vibrational mode i in a PAH population is given by

$$I_i = \sum_j \sum_Z n_j \sigma_{ij}(Z) f_j(Z) \int_{2.7\ \mathrm{K}}^{T_{\max}} B_\nu G_j(T) dT \ , \qquad (1)$$

where n_j is the number density of the j^{th} PAH, $\sigma_{ij}(Z)$ is the IR cross section of mode i in the j^{th} PAH with charge Z in the composite population, $f_j(Z)$ is the fraction of that PAH at charge Z, $T_{\max}$ is the maximum vibrational temperature attained by the PAH upon absorption of a photon, B_ν is the Planck function, and $G_j(T)$ is the temperature probability distribution of the j^{th} PAH. Using this treatment, we can produce the composite interstellar IR emission spectrum expected for distinct families of PAHs (characterized by their molecular structure) in a variety of interstellar regions in order to compare how well each family matches to astrophysical observations.

2.2. *The IR Spectral Characteristics of the Interstellar PAH Family*

The interstellar IR emission spectral profile from a range of ISM conditions can vary depending on the charge, molecular structure, size, and degree of hydrogenation of the carriers, as well as whether or not they have molecular sidegroups attached. In particular, the PAH charge plays a significant role in the relative intensities of the IR emission bands (e.g., Szczepanski & Vala 1993; Hudgins & Allamandola 1995; Langhoff 1996; Joblin et al. 1996; BTB2001). Here we combine the absolute and relative band intensities of ionized PAHs, which have been determined by the Ames Computational Chemistry Group and the Ames Astrochemistry Laboratory and have been incorporated into a comprehensive PAH IR spectral database. At present, relative band intensities of neutral and ionized PAHs composed of between 10 and 96 atoms have been determined. There are now over 80 different PAH species in this database, including spectra of neutral, cationic, and anionic PAHs. These PAHs can be hydrogenated, dehydrogenated, and have sidegroups and isotopic substituents. Band positions and relative band intensities provide a firm foundation for our model of PAH IR emission. As the PAH IR spectral database expands, the model will be updated. We can use the spectral database to help constrain the carriers of the interstellar IR emission features between 3.3 and 25 μm and track their evolution as they coevolve with the changing environment of the ISM.

Figures 1*a* and 1*b* illustrate the good match between the laboratory database and the quantum chemical calculations of Bauschlicher (2000)[1] for a set of PAHs ranging from naphthalene $C_{10}H_8$ to dicoronylene $C_{48}H_{18}$. We have chosen a wide variety of sizes and molecular structures in order to give the reader an overview of the extensive sample of PAHs available within the database and to allow a fair comparison of how well theoretical and laboratory spectra match. Because the IR fluorescence spectrum is governed by the relative strength of the IR bands, these spectra are normalized by the total integrated IR cross section for ease of comparison between each PAH species.

The calculated and measured IR cross sections of neutral PAHs agree on average to within ~ 4 cm^{-1} for the peak position and 15% in the intensity of individual features between the theoretical calculations of Bauschlicher & Langhoff (1997) and the experimental work of Szczepanski and Vala (1993) and Hudgins, Sandford, & Allamandola

[1] C. W. Bauschlicher 2000, Online Spectral Database; see http://ccf.arc.nasa.gov/~cbauschl/.

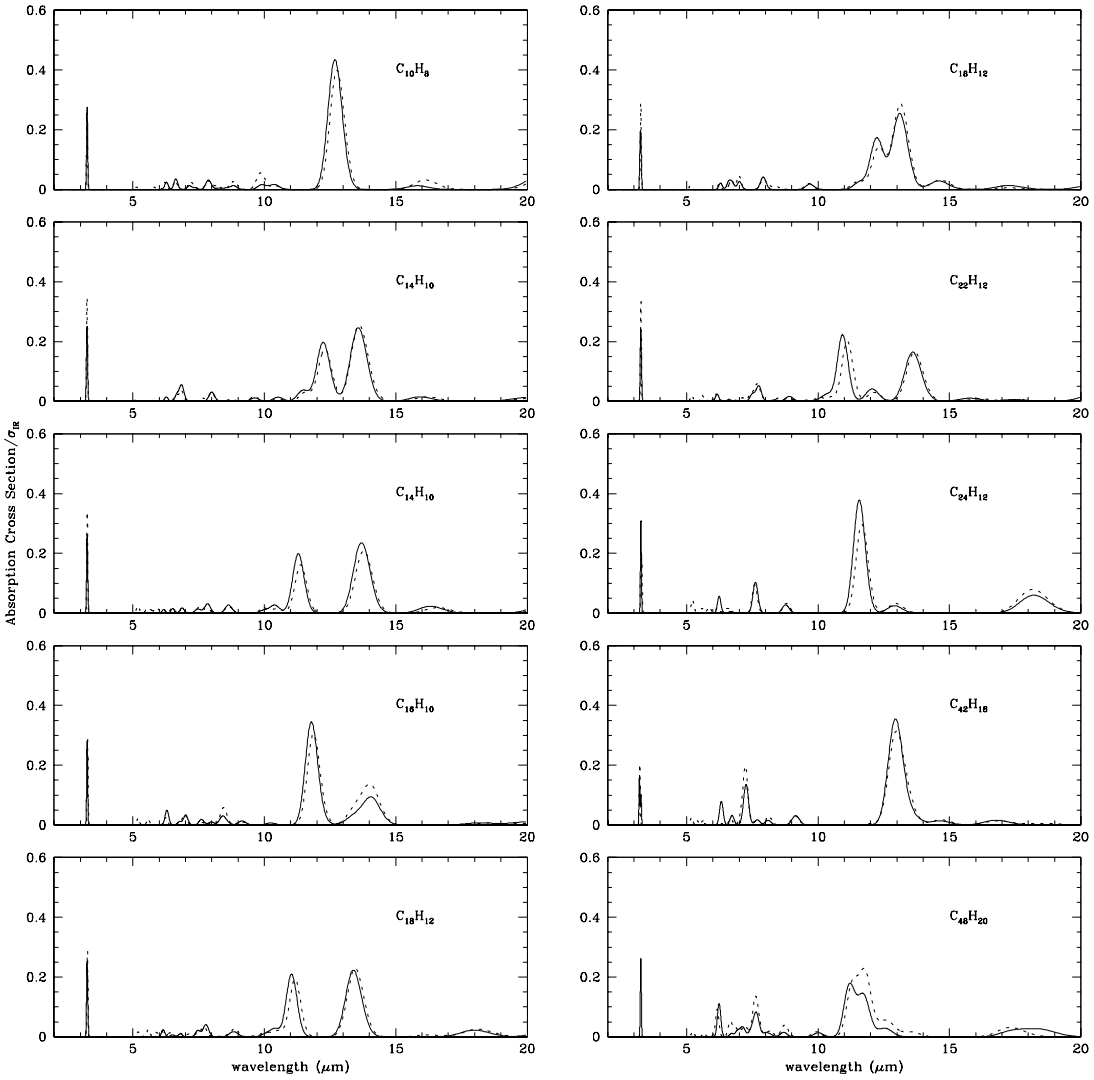

Fig. 1*a*

FIG. 1.—(*a*) Excellent match between the quantum chemically calculated (*solid line*) and the laboratory measured (*dashed line*) IR cross sections for neutral naphthalene $C_{10}H_8$, anthracene and phenanthrene $C_{14}H_{10}$, pyrene $C_{16}H_{10}$, tetracenene and chrysene $C_{18}H_{12}$, pentacene $C_{22}H_{14}$, coronene $C_{24}H_{12}$, hexabenzocoronene $C_{42}H_{18}$, and dicoronylene $C_{48}H_{20}$. (*b*) Same as Fig. 1*a*, but for singly charged cationic PAH species. The match between the quantum chemically calculated (*solid line*) and the laboratory measured (*dashed line*) IR cross sections is mostly very good and is within the acceptable range of errors.

(1994). The theoretically calculated 3.3 μm band strength is systematically larger than the measured strength and has therefore been uniformly reduced in strength for all PAHs by a factor of 2 (see Langhoff 1996 for details) before this comparison was made. For the cations, the match is not as good as for the neutrals. The peak position agrees on average to within 14 cm^{-1}, but the relative strength differs now by over 15%. For a few bands of a limited number of cationic PAHs, the difference in strength can amount to a factor of 2. For the total integrated intensity under the IR spectral profile for both neutrals and cations, we find a less than 1% difference between the quantum chemically calculated PAH IR cross sections and those measured in the laboratory. Finally, while spectra of doubly charged and triply charged PAHs have been theoretically calculated because they are relevant to highly UV irradiated regions such as the Orion PDR, no laboratory spectra of such species are yet available. Hence, we have decided to consistently rely on the theoretical values for peak positions and band strengths for all charge states. In the following evaluations, the variations illustrated by Figures 1*a* and 1*b* should be kept in mind.

Perusal of Figures 1*a* and 1*b* shows that neutral PAHs display a strong feature at 3.3 μm owing to the C–H stretching mode but have very weak C–C modes in the 6–9 μm region (Langhoff 1996; Hudgins et al. 1999a, 1999b). Neutrals also display features longward of 11.0 μm caused by out-of-plane (OOP) C–H bending modes, which have a characteristic pattern reflecting the number of adjacent H atoms on the rings (Verstraete et al. 1996; Hony et al. 2001). In contrast, PAH cations display strong features in the 6.2–9 μm region, while their activity in the 3.3 μm band and wavelengths longer than 11.0 μm is depressed. This reflects the increased activity of the C–C skeletal modes relative to the C–H modes, owing to the presence of extra charge in the PAH structure. As emphasized in Paper I, the C–C modes

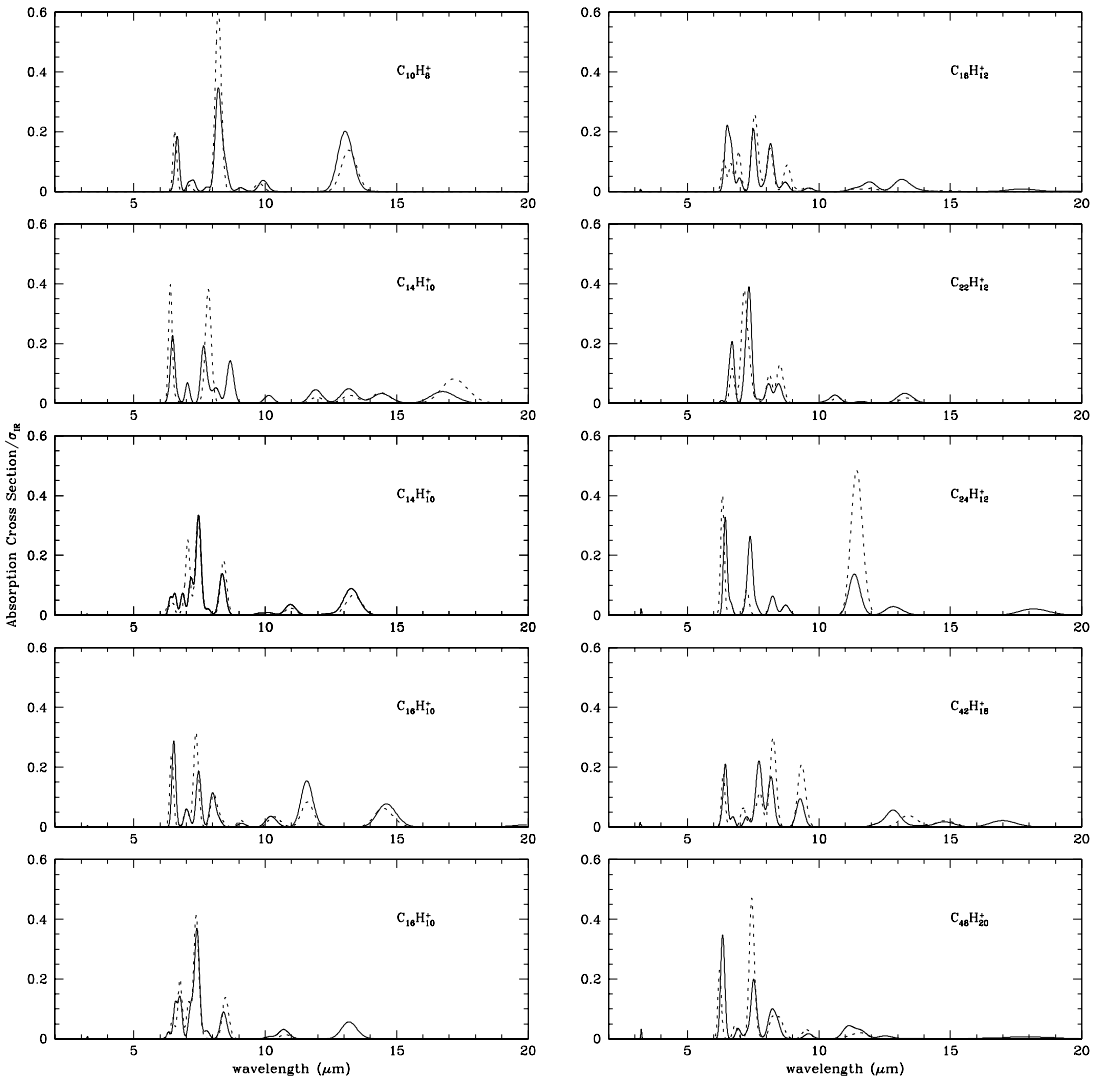

Fig. 1*b*

become ever more pronounced compared to the C–H modes in multiply charged PAHs. Anionic PAHs, on the other hand, combine the IR characteristics of neutral PAHs (strong C–H modes) with those of cationic PAHs (strong C–C modes).

For this paper, we have divided PAHs in this sample into symmetric condensed, symmetric noncondensed, linear, methylated, and PAHs containing pentagonal rings (Table 1) and calculated the variation of their charge state and the resulting IR emission spectra for different regions of the ISM. This provides a foundation to predict and explore the effects of molecular structure on the IR spectrum of PAHs in the ISM as the UV field and electron density change. The PAH charge is determined by a balance between photoelectrically ejected electrons and PAH-electron recombination (BT94). This balance depends on the ratio of the illuminating UV radiation field (measured in Habing units of G_0) and the electron density n_e. In order to quantify this effect, we have studied the parameter space of $1 < G_0/n_e < 10^5$ appropriate for interstellar regions ranging from the diffuse ISM to dense PDRs associated with regions of massive star formation.

3. THE EFFECTS OF PAH MOLECULAR STRUCTURE ON THE IR EMISSION SPECTRUM

We discuss the general effects of molecular structure in detail for our different classes of PAHs below. In the figures below, which cover an extensive range of G_0/n_e, bear in mind that for typical diffuse clouds ($G_0 = 1$; $n_{\rm H} = 20$ cm^{-3}), $G_0/n_e \sim 500$. For reflection nebulae such as NGC 2023 ($G_0 = 10^4$; $n_{\rm H} = 10^5$ cm^{-3}), $G_0/n_e \sim 10^3$, while for PDRs associated with H II regions such as the Orion bar ($G_0 = 4 \times 10^4$; $n_{\rm H} = 5 \times 10^4$ cm^{-3}), $G_0/n_e \sim 10^4$. In addition, we take all PAHs as having an equal abundance in each of our different classes. Furthermore, when we mix each class together to form a composite population of PAHs, we adhere to this 1:1 ratio for simplicity. However, in the general ISM, this is probably not the case. We leave the study of this effect to a later paper in the series.

3.1. *Symmetric Condensed PAHs*

Because all bonds have equal strength for symmetric PAHs, there are no "weak links," and multiple bonds have to be broken to disrupt their molecular structure. For a

given size, the most symmetric PAH structures are thus thought to be the most thermodynamically stable PAH species. This class of PAHs has been extensively discussed in Paper I (BTB2001), and the corresponding symmetric PAH spectrum is overlaid as a dashed line on subsequent classes of spectra for different members of the PAH family for comparison. In brief, for low G_0/n_e ($\leq 10^3$ cm^3), the PAH charge distribution will be dominated by the lowest charge attainable (neutral or anionic). The PAHs will lose electrons and for $G_0/n_e \sim 10^4$ or higher, the charge distribution will be skewed toward the highest attainable positive charge. As G_0/n_e increases, the PAH features at 3.3 and 11.2 μm undergo a dramatic decrease as G_0/n_e increases above 10^3. This reflects a shift in their charge state. Hence, we conclude (from Paper I) that neutral and anionic PAHs dominate the emission in the 3.3 and 11.2 μm features (C–H modes). In contrast, the ions dominate the C–C modes (6.2–9 μm), and as G_0/n_e increases further, the multiply charged cationic states emerge as the ionizing UV radiation photoelectrically ejects further electrons from the +1 charge state. The OOP bending modes in the 11–15 μm region have a characteristic pattern that reflects the number of adjacent H atoms on the rings (Bellamy 1975; Hudgins et al. 2001). This pattern changes somewhat upon ionization (Hudgins & Allamandola 1999a, 1999b; Hony et al. 2001).

At $G_0/n_e > 10^3$, cations emerge as the dominant PAH species, and the presence of one or more charges enhances the strength of the C–C stretching modes between 6.2 and 9 μm, an effect that increases with the number of carbon atoms in the PAH (Langhoff 1996). The strength of the C–C modes is even more enhanced for multiply charged PAHs. In addition, the 3.3 μm C–H stretching mode is very weak, and the OOP bending modes in the 11–15 μm region carry typically less than 10% of the integrated intensity over all bands. Multiply ionized PAHs show the same general trends as singly ionized PAHs in their emission characteristics. There is a shift in the peak position of the IR bands as both the charge and the size of the PAH increases. For the C–C modes, ionization at constant PAH size shifts the 6.2 μm feature to longer wavelengths, while increasing PAH size with constant ionization generally shifts this feature to shorter wavelengths for this particular sample of PAHs, until for $C_{54}H_{18}^+$, the wavelength of this feature shifts back slightly to longer wavelengths. Further studies involving larger PAHs should be performed to determine the true nature of these shifts and their variation with PAH size, charge, and geometry.

3.2. *Symmetric Noncondensed PAHs*

The main differences between the symmetric condensed population and the symmetric noncondensed population (Fig. 2) is the relative absence of emission in the 6.2–9 μm region and the presence of a double-peaked feature longward of 11 μm (OOP modes) for low values of G_0/n_e (1–10^3 cm^3). The lack of emission in the 6–9 μm region is due to the fact that for low G_0/n_e, emission in this wavelength region derives mainly from anions, and the only PAH in this population that can easily acquire an electron is triphenylene. All the other small PAHs in this set of symmetric noncondensed PAHs have low-electron affinities and small electron sticking coefficients (ATB98). As a result, emission in the 6–9 μm region is small relative to the emission from the rest of the neutral PAH population at 3.3 μm and longward of 11 μm. Hence, this difference is to a large extent a selection effect, since only small symmetric noncondensed PAHs have presently been studied in the laboratory or via quantum chemistry. The double peak in the emission longward of 11 μm is due to blended emission from duo (two adjacent H atoms) and trio (three adjacent H atoms) modes from both anionic and neutral members of this population. This differs significantly from the symmetric condensed PAH emission, which contains mainly solo modes around 11.2 μm. For $G_0/n_e = 10^3$, the major portion of the emission originates from the neutrals, with a charge transition at $G_0/n_e = 10^4$, where the emission mainly originates from singly charged cations and a smaller proportion of neutrals. At $G_0/n_e = 10^5$, the emission originates from singly and doubly charged cations with virtually no contribution from the neutral species. Around $G_0/n_e = 10^3$, the symmetric condensed emission and the symmetric noncondensed emission in the 6–9 μm region begin to look more similar, an effect that increases with G_0/n_e. The emission from the 3.3 μm region and the region longward of 11.0 μm is severely depressed at high G_0/n_e, since these features originate from neutral and anionic PAHs.

Differences in the peak position of the IR features between 6.2 and 8.6 μm with molecular structure at higher G_0/n_e ($\geq 10^3$) are apparent, since for symmetric condensed PAHs, the 6.2 μm feature is situated at a shorter wavelength than that for symmetric noncondensed PAHs. As G_0/n_e increases to 10^5, the 6.2 μm feature for both classes of PAH

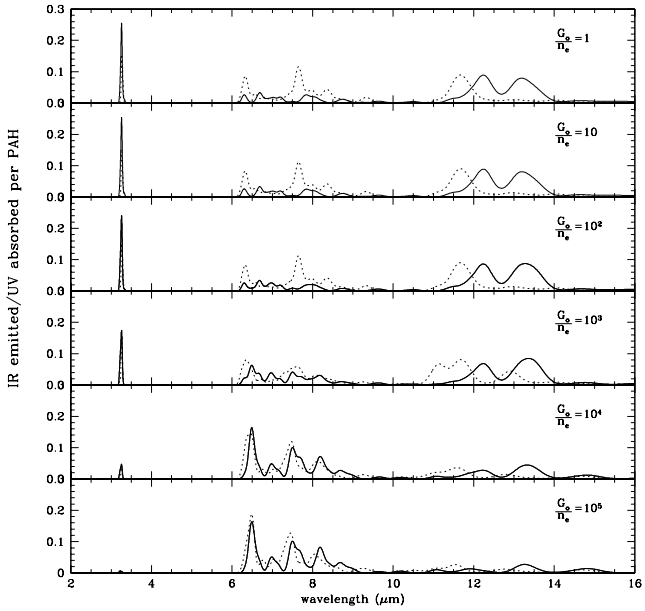

FIG. 2.—Comparison of the IR emission spectra of the symmetric condensed population (*dashed line*) and the symmetric noncondensed population (*solid line*) for a wide range of interstellar conditions. The relative absence of emission in the 6.2–9 μm region is due to the fact that for low G_0/n_e, emission derives mainly from anions, and the only anion in this population that has a high abundance is triphenylene. This is an artificial selection effect of our sample size, since only small symmetric noncondensed PAHs have been studied via quantum chemistry and the laboratory. The double peak in the emission longward of 11 μm is due to blended emission from duo (two adjacent H atoms) and trio (three adjacent H atoms) modes from both anionic and neutral members of this population. For $G_0/n_e = 10^3$, the major portion of the emission originates from the neutrals, with a charge transition at $G_0/n_e = 10^4$, where the emission mainly originates from singly charged cations and a smaller proportion of neutrals. At $G_0/n_e = 10^5$, the emission originates from singly and doubly charged cations with almost no contribution from the neutral species.

converge to the same peak position. The 7.7 μm feature is minimal for symmetric noncondensed PAHs until $G_0/n_e \geq 10$, after which it increases in intensity and shifts its peak position to slightly shorter wavelengths with increasing G_0/n_e.

3.3. *Linear PAHs*

Linear PAHs are not expected to be as robust as symmetric condensed PAHs because their linear structure is more vulnerable to unimolecular dissociation upon absorption of high-energy photons. Figure 3 illustrates their IR spectral variation with varying G_0/n_e. For $G_0/n_e = 1$ and 10, naphthalene, tetracene, and pentacene anions predominate, giving rise to activity in all salient wavelength regions from 3.3 to 11.2 μm and longward of 12.7 μm. However, the 6.2 μm feature apparent for symmetric condensed PAHs is shifted to 6.6 μm, the 7.7 μm feature is shifted to 7.5 μm, and the 8.6 μm feature is shifted to 8.4 μm for linear PAHs. The 11.2 μm feature is small relative to its "counterpart" for symmetric PAHs because the quartet modes (four adjacent H atoms) longward of 12.7 μm take up an appreciable fraction of the OOP emission. Around $G_0/n_e = 10^2$, neutrals predominate, and the activity between 6 and 9 μm is suppressed relative to the neutral bands at 3.3 μm and wavelengths longward of 11.2 μm. The double peak around 3.3 μm is due to a blend of anionic features around 3.26 and 3.3 μm, and this blended feature gradually shrinks as neutrals begin to predominate. As G_0/n_e increases from 10^3 to 10^4, the cationic charge state +1 predominates, with the accompanying increase in the intensity of the 6.2–9 μm features and a decrease in the 3.3 μm and 11.2 μm emission. At $G_0/n_e = 10^5$, the cationic charge states +1 and +2 predominate, and the neutral emission is completely suppressed. While most pronounced at low G_0/n_e, the shift in the wavelength of the IR features between 6 and 9 μm relative to those for symmetric condensed PAHs is apparent for all G_0/n_e.

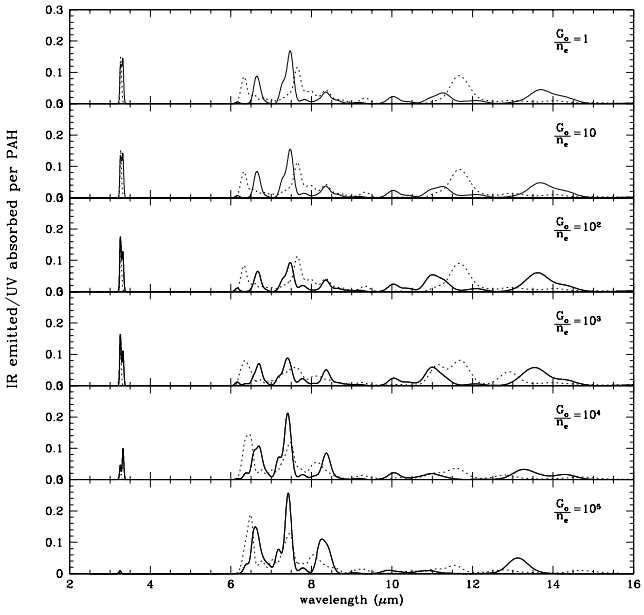

FIG. 3.—Comparison of the IR emission spectra of the symmetric condensed population (*dashed line*) and the linear population (*solid line*) for a wide range of interstellar conditions. For $G_0/n_e = 1$ and 10, naphthalene, tetracene, and pentacene anions predominate, giving rise to activity in all salient wavelength regions from 3.3 to 11.2 μm and longward of 12.7 μm. At $G_0/n_e = 10^2$, neutrals predominate, and the activity between 6.2 and 9 μm is suppressed relative to the neutral bands at 3.3 μm and wavelengths longward of 11.2 μm. The double peak around 3.3 μm is due to a blend of anionic features at 3.26 and 3.3 μm. As G_0/n_e increases from 10^3 to 10^4, the cationic charge state +1 predominates, with the expected increase in the intensity of the 6.2–9 μm features and a decrease in the 3.3 μm and 11.2 μm emission. At $G_0/n_e = 10^5$, the cationic charge states +1 and +2 predominate, and the neutral emission is suppressed. The feature at 13 μm reflects characteristic emission mode for four adjacent H atoms.

3.4. *PAHs Containing Pentagonal Rings*

It has been suggested that PAHs containing pentagonal rings are an important molecular intermediary on the route to the formation of large interstellar molecules (Frenklach & Feigelson 1989; Beegle et al. 1997; Marinov et al. 1998). These PAHs do not form anions in the variety of ISM studied in this paper and occupy only the neutral and cationic charge states. This means that for low G_0/n_e, only the neutral form contributes to the interstellar IR emission. Interestingly, there is still a distinct feature at 7.0 μm despite the absence of anions at low G_0/n_e (Fig. 4). The 7.0 μm feature arises mainly from in plane C–H bending modes with a smaller component of C–C stretching arising from the asymmetry introduced into the PAH structure by the pentagonal ring. The stronger the 7.0 μm feature, the more asymmetric the PAH structure. Also, emission longward of 11.0 μm shows blended emission from solo (11.2 μm), duo (12.0 μm), and trio (12.7 μm) modes of hydrogen. At $G_0/n_e = 10^3$, the cationic +1 state arises, leaving its characteristic signatures between 6 and 9 μm. In addition, at $G_0/n_e \geq 10^3$, we see the characteristic decrease in the neutral emission at 3.3 μm and longward of 11.2 μm and

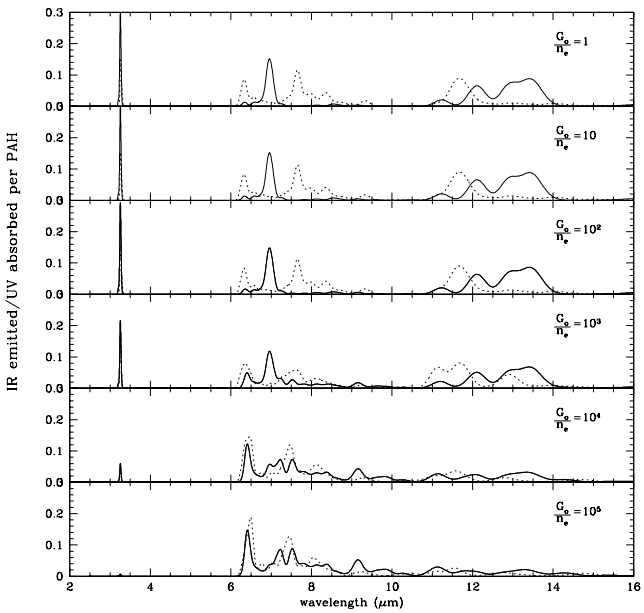

FIG. 4.—Comparison of the IR emission spectra of the symmetric condensed population (*dashed line*) and the pentagonal ring containing PAH population (*solid line*) for a wide range of interstellar conditions. These PAHs do not form anions and occupy the neutral and cationic charge states. For low G_0/n_e, only the neutral form contributes to the interstellar IR emission. Emission longward of 11.0 μm shows blended emission from solo (11.2 μm), duo (12.0 μm), and trio (12.7 μm) modes of hydrogen. As G_0/n_e increases to 10^3, the cationic +1 state arises, leaving its characteristic signatures between 6.2 and 9 μm, and we see a corresponding decrease in the neutral emission at 3.3 μm and longward of 11.2 μm.

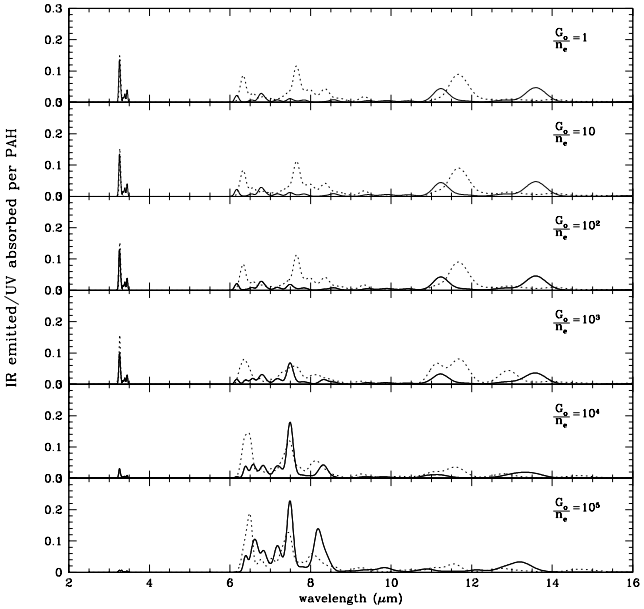

FIG. 5.—Comparison of the IR emission spectra of the symmetric condensed population (*dashed line*) and the methylated PAH population (*solid line*) for a wide range of interstellar conditions. A 3.4 μm feature characteristic of methylated PAHs can be seen shadowing the usual 3.3 μm C–H stretch feature. The spectra show all the trends of the other classes of PAHs—the inevitable decline of the 3.3 μm and OOP modes features with increasing G_0/n_e, signaling the predominance of cations over neutrals and anions, plus the corresponding increase in the 6.2–9 μm features. The active OOP modes at low G_0/n_e indicate the presence of solo and trio C–H stretch modes longward of 11.0 μm. As G_0/n_e increases, the C–C stretch modes kick in, producing characteristic emission between 6.2 and 9 μm with the corresponding suppression of the neutral emission at 3.3 μm and longward of 11.0 μm. Currently, we have only been able to study the smaller species with only one ionization potential; hence, these spectra describe only the +1 cationic state. In the future, we hope to expand the size of this sample.

conversely, an increase in the cationic emission between 6 and 9 μm. Finally, we see band shifts for the 6.2, 7.7, and 8.6 μm features at higher G_0/n_e, as the 6.2 μm features shifts to 6.4 μm and the "7.7" μm band becomes a double-peaked feature at 7.2 and 7.5 μm.

3.5. *Methylated PAHs*

The 3.4 micron feature—a weak satellite band to the strong 3.3 micron aromatic CH stretching mode in some sources—is generally attributed to the CH stretching mode of CH_3 groups attached to PAH molecules (Joblin et al. 1996). Of course, the 3.4 μm band may arise from different carriers. For instance, the overtone of the aromatic C–H stretch vibration ($v = 2$ to $v = 1$; Barker, Allamandola, & Tielens 1987) in a population of very small PAHs. This is a complex problem, and it is not within the scope of this paper to adequately cover the numerous suggested carriers. However, here we can address the complete mid-IR spectrum of linear methylated PAHs and compare with their "parent" population. The 3.4 μm C–H stretch owing to the methyl group can be seen clearly in Figure 5. The weakness of the C–C modes for low G_0/n_e is apparent, and this is due to the paucity of anionic species in this population and may be a selection effect of our sample. The spectra show all the trends of the other classes of PAHs—the inevitable decline of the 3.3 μm and OOP modes features with increasing G_0/n_e, signaling the predominance of cations over neutrals and anions, plus the corresponding increase in the 6–9 μm features. The active OOP modes at low G_0/n_e indicate the presence of solo, trio, and quartet C–H stretch modes longward of 11.0 μm. While the solo mode remains centered around 11.2 μm, the trio and quartet modes, which normally occupy the 12.7 μm peak position have shifted longward of 13 μm. In addition, as G_0/n_e increases, this feature shifts from 13.6 to 13.2 μm, reflecting the shift in the charge

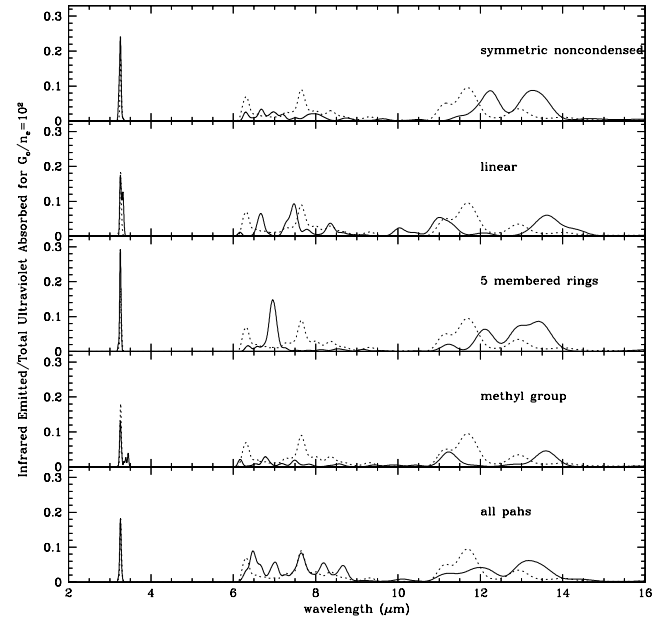

Fig. 6*a*

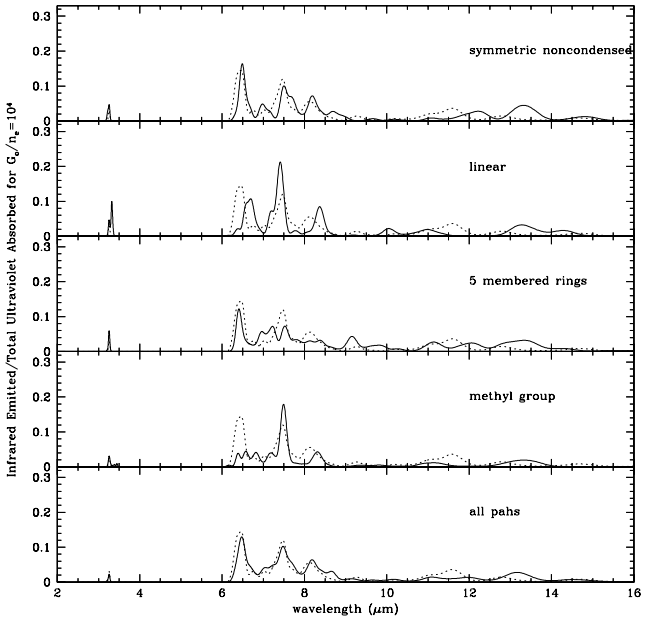

Fig. 6*b*

FIG. 6.—(*a*) Expected variation in the IR emission features for each class of PAH plus the combination of all of these classes for $G_0/n_e = 10^2$, while (*b*) shows the same for $G_0/n_e = 10^4$. The dashed line represents the symmetric PAH population studied for comparison with the population taken from Paper I. Panel (*a*) illustrates how very different the IR emission spectrum for each class of PAHs is for low G_0/n_e, where neutrals and anionic PAHs dominate the PAH charge distribution. However, as (*b*) illustrates, the IR spectral profiles of the five different classes of PAHs resemble each other at higher G_0/n_e. The reader should bear in mind that for the general ISM bathed in a high UV field ($G_0 = 10^5$), the more robust symmetric condensed species may predominate, while for H II regions with an even higher UV field, PAHs may be partially destroyed or irregular.

distribution of the PAHs, from anionic to neutral to cationic. The spectral profiles do not much resemble those of symmetric condensed PAHs over the entire range of G_0/n_e, which we expect because our sample of methylated PAHs is limited to a linear molecular structure only. The best match to the symmetric condensed PAHs is at $G_0/n_e = 10^5$. The qualitative spectral differences of methylated PAHs relative to symmetric, condensed PAHs are much like those described for linear PAHs above. In the future, we will expand our database to include a more diverse population of molecular structures for methylated PAHs.

3.6. *Varying G_0/n_e for our Entire PAH Population*

Figures 6*a* and 6*b* show the expected variation in the IR emission features for each class of PAH plus the combination of all of these classes for $G_0/n_e = 10^2$ and $G_0/n_e = 10^4$, respectively. For comparison, the dotted line represents the symmetric PAH population (Paper I). Figure 6*a* illustrates how very different the IR emission spectrum for each class of PAHs is at low G_0/n_e, where neutrals and anionic PAHs dominate the PAH charge distribution. This is partly a function of our sample size for each classification of PAH, since this paper concentrates on smaller PAHs ($N_c < 32$) owing to the lack of availability of larger species in our database. In general, the smaller PAHs in our classes do not have high-electron affinities and have little chance of attaining a negative charge as a result. This lack of anions results in a pronounced difference in the spectral profiles of each class at low G_0/n_e. Because there is a significant shift in the peak position of the IR emission features relative to the symmetric, condensed PAHs, this means that the IR spectra are effective diagnostics of the molecular structure of the interstellar PAH family for low radiation field to electron density ratios. However, as Figure 6*b* illustrates, the IR spectral profiles of the five different classes of PAHs resemble each other much more for higher G_0/n_e. Each PAH in each different class was added into the composite spectrum assuming an equal abundance for simplicity. However, this is likely not the case for the general ISM, where for high UV fields ($G_0 = 10^5$), only the more robust, symmetric species predominate, while for H II regions with an even higher UV field, PAHs may be partially destroyed or have an irregular structure owing to photoerosion.

4. VARIATION OF THE MODEL SPECTRUM FOR THE ORION PDR

4.1. *The IR Spectrum at the Orion PDR Surface*

PDRs are bright in the well-known PAH IR emission features between 3.3 and 12.7 μm. At the PDR surface, the high-UV flux means that the photoelectric ejection of electrons dominates PAH charging. The BTB2001 model can account for the relative strength of the C–C and C–H modes owing to the dominant presence of singly and multiply charged PAH cations, with a very small fraction of neutrals. In addition to the PAH charge state having a significant effect on the IR spectral profile emerging from the Orion PDR, molecular structure also exerts a strong influence on the resulting IR emission. We investigate the effects of these two factors for the Orion PDR. Figure 7 illustrates the IR emission profile for symmetric condensed, symmetric noncondensed, linear, pentagonal rings, and methyl group–containing PAHs, with the top panel providing a comparison to *ISO* observations of the Orion PDR

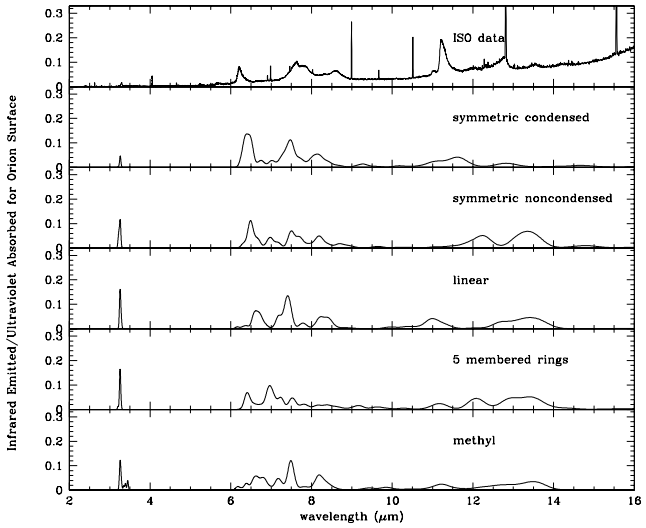

FIG. 7.—IR emission profile for symmetric condensed, symmetric noncondensed, linear, pentagonal rings, and methyl group–containing PAHs at the Orion PDR surface. Each profile is distinct and shows variations in the peak position and intensity of the typical interstellar IR emission features at 3.3, 6.2, 7.7, 8.6, 11.2, and 12.7 μm. The top panel is *ISO* data taken from observations of the surface of the Orion PDR for comparison.

surface. Each profile is distinct and shows variations in the peak position and intensity of the typical interstellar IR emission features at 3.3, 6.2, 7.7, 8.6, 11.2, and 12.7 μm. The most satisfactory match to observational data from *ISO* comes from the symmetric condensed PAHs. From all the PAHs considered here, symmetric condensed PAHs fit best. Those PAHs are also thought to survive best in the harsh conditions of the Orion PDR (ATB89; Schutte et al. 1993; BTB2001). However, we emphasize that our comparison has built in selection effects owing to the PAH families studied in the laboratory and quantum chemical databases. As the databases expand in the future to include broader classes of PAH molecular structure (e.g., asymmetric/irregular, partially eroded, and so on) and larger PAHs, these selection effects will diminish.

4.2. *Spatial Variation of the Model Spectrum for the Orion PDR*

Figure 8 illustrates the dependence of the interstellar IR emission spectrum as a function of depth (A_v) into the PDR. The PAH population in this calculation contains all five classes of PAHs. For comparison, the symmetric condensed PAH profile from the population studied in Paper I is shown as a dashed line. The PAH IR emission is normalized to the total UV absorbed. However, for the IR emission taken by itself, the absolute intensity drops with depth A_v into the PDR by a factor $e^{-1.8\ A_v}$ as the UV radiation is attenuated, and Figure 8 is simply meant to illustrate the change in the IR spectral profile with depth. The incident UV field determines the PAH charge balance, which in turn determines the profile with depth into the PDR. At the PDR surface ($A_v = 0$), multiply and singly charged PAH cations, with a very small fraction of neutrals, dominate the emission. This is exhibited via the dominance of the 6–9 μm region over the 3.3 μm feature and the OOP modes longward of 11.0 μm. Deeper into the PDR, as A_v increases and the UV flux is attenuated, the PAHs become neutral and negatively charged. As the neutrals and anions begin to

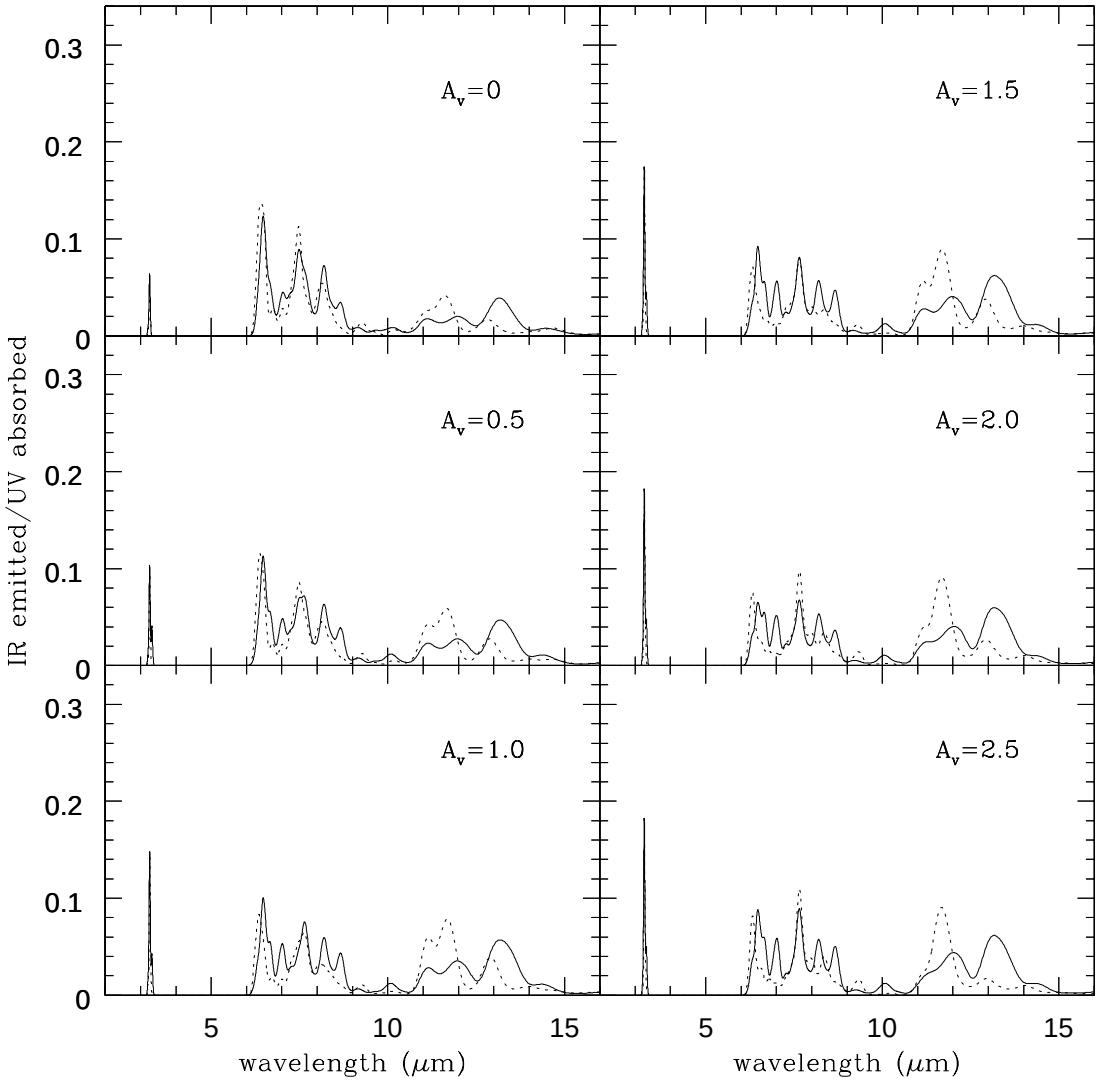

FIG. 8.—Interstellar IR emission profile for a population containing all five classes of PAHs studied in this paper for the Orion PDR, normalized to the UV radiation absorbed. For comparison, the symmetric condensed PAH profile from the population studied in Paper I is shown as a dashed line. The incident UV field is attenuated with depth into the PDR by a factor $e^{-1.8 A_v}$ and this controls the charge balance, which, in turn, determines the profile with depth into the PDR. At the PDR surface ($A_v = 0$), the presence of multiply and singly charged PAH cations, with a very small fraction of neutrals, dominates the emission via photoelectric ejection of electrons from the PAHs. This is exhibited via the dominance of the 6–9 μm region over the 3.3 μm feature and the OOP modes longward of 11.0 μm. Deeper into the PDR, as the UV flux is attenuated, PAHs become neutral and negatively charged. As the neutrals and anions begin to dominate over cations deeper into the PDR ($A_v \sim 1$–1.5), the IR spectral profile changes, with the 3.3 μm feature dominating over the rest of the IR spectrum and the OOP modes longward of 11.0 μm increasing in overall intensity.

dominate over cations, the IR spectral profile changes for features between 3.3 and 12.7 μm, with the 3.3 μm feature dominating over the rest of the IR spectrum and the OOP modes longward of 11.0 μm increasing in overall intensity.

Figure 8 illustrates these preliminary results for the Orion PDR, and, clearly, PAH charge, size, and molecular structure exert a dramatic effect on the resulting spectral profile and its evolution throughout an interstellar region. PAH size and structure comes into play with the addition of other classes of PAHs (many of a size less than 30 carbon atoms) to our PAH population of symmetric condensed PAHs in Paper I. This increases the strength of the 3.3 μm feature relative to the other PAH IR emission features, and it alters the characteristic profile of the OOP modes longward of 11.0 μm by adding in more duo and trio modes for H atoms attached to the PAHs. In addition, adding other classes of PAH damps down the solo H atom OOP mode relative to its sister OOP modes. Finally, the general profile of the 6–9 μm region changes when classes of PAHs other than symmetric condensed PAHs are added to our population via the appearance of a feature at 7.0 and 8.8 μm. However, we note that it is still the PAH charge that exerts the most dramatic effect on the interstellar IR emission spectrum of the PDR. In Paper III, we will make a more in-depth study of the Orion PDR, its IR emission spectrum, and its hydrogen chemistry and compare our results with relevant observational data. In addition, the results of this and following papers that highlight subtle changes in band position with molecular structure will be used to interpret data from future space borne observatories. Results in this paper concern the variation of, for example, the 3.3/6.2 μm ratio, which acts as a diagnostic of both carrier size and degree of ionization. Space and airborne observatories are the only window we have on the 6.2 μm feature, which traces the

emergence of cationic and anionic PAH species at low resolution. As such, there is much work remaining to be done via the investigation of its variation with depth into a star-forming region, following *ISO* observations of this feature (Pierre et al. 1996; Verstraete et al. 1996).

5. CONCLUSIONS

The molecular structure of the PAH population exerts a significant effect on the IR spectral profile of interstellar regions at lower G_0/n_e. The resulting spectrum arising from each population is unique, and it is easy to tell emission arising from one class of PAH to another by looking at the distinct shape of the 3.3 μm (linear PAHs) or 3.4 μm feature (methylated PAHs) or the distinctive OOP modes (solo, duo, or trio) longward of 11.0 μm. At higher G_0/n_e, the IR emission becomes less differentiated in the 6–9 μm region from class to class, but the intensity and shape of the 3.3 μm region and emission longward of 11.0 μm, although depressed relative to the 6–9 μm region, becomes one way of diagnosing the predominant class of IR emitters. Broadly speaking, for the PAH molecular structures studied in this paper, it is the symmetric condensed PAHs, which can reach multiple charge states that dominate at high G_0/n_e. At lower G_0/n_e, symmetric condensed PAHs may dominate the emission, but we can effectively diagnose this from the fine structure of the IR emission features between 3.3 and 12.7 μm, because each class of PAHs in this parameter space of interstellar conditions produces a very distinct IR spectral signature. However, it is the charge state that exerts the most significant effect on the PAH IR emission spectrum, more significant than the molecular structure of the five classes of PAHs studied in this paper. Finally, it is necessary to broaden the sample of PAHs in our databases to include more molecules larger than 30 carbon atoms, in order to create a more representative interstellar PAH population in our model. In addition, it is of interest to study the effects of the PAH hydrogenation state on the resultant IR emission spectrum in star-forming regions, and this will form the basis of our next paper.

E. L. O. B. thanks the NASA Astrophysics Theory Program for their financial support of the work in this paper. We thank Els Peeters for her generous donation of *ISO* data covering the surface of the Orion PDR.

REFERENCES

Allamandola, L. J., Tielens, A. G. G. M., & Barker, J. R. 1985, ApJ, 290, L25 (ATB85)
———. 1989, ApJS, 71, 733 (ATB89)
Bakes, E. L. O. 1992, Ph.D. thesis, Univ. London
Bakes, E. L. O., & Tielens, A. G. G. M. 1994, ApJ, 427, 822 (BT94)
Bakes, E. L. O., Tielens, A. G. G. M., & Bauschlicher, C. W. 2001, ApJ, 556, 501
Barker, J. R., Allamandola, L. J., & Tielens, A. G. G. M. 1987, ApJ, 315, L61
Bauschlicher, C., & Bakes, E. L. O. 2000, Chem. Phys., 262, 285
Bauschlicher, C. W., & Langhoff, S. 1997, Spectrochim. Acta, 53, 1225
Beegle, L. W., Wdowiak, T. J., Robinson, M. S., Cronin, J. R., McGehee, M. D., Clemett, S. J., & Gillette, S. 1997, ApJ, 487, 976
Bellamy, L. J. 1975, Infrared Spectra of Complex Molecules (London: Chapman & Hall)
Brenner, J., & Barker, J. R. 1992, ApJ, 388, L39
Chercheneff, I., & Barker, J. D. 1989, ApJ, 341, L21
Cook, D. J., & Saykally, R. J. 1998, ApJ, 493, 793
Désert, F.-X., Boulanger, F., & Puget, J. L. 1990, A&A, 237, 215
Draine, B. T., & Anderson, N. 1985, ApJ, 292, 494
Frenklach, M., & Feigelson, E. D. 1989, ApJ, 341, 372
Hony, S., van Kerckhoven, C., Peeters, E., Tielens, A. G. G. M., Hudgins, D. M., & Allamandola, L. J. 2001, A&A, 370, 1030
Hudgins, D. M., & Allamandola, L. J. 1995, J. Chem. Phys., 99, 3033
———. 1999a, ApJ, 516, L41
———. 1999b, ApJ, 513, L69
Hudgins, D., Bauschlicher, C., & Allamandola, L. J. 2001, Spectrochim. Acta, 57, 907
Hudgins, D. M., Sandford, S. A., & Allamandola, L. J. 1994, J. Phys. Chem., 98, 4243
Joblin, C., Tielens, A. G. G. M., Allamandola, L. J., & Geballe, T. R. 1996, ApJ, 458, 610
Langhoff, S. R. 1996, J. Phys. Chem., 100, 2819
Léger, A., & Puget, J. L. 1984, A&A, 137, L5
Marinov, N. M., Pitz, W. J., Westbrook, C. K., Vincitore, A. M., Castaldi, M. J., Senkan, S. M., & Melius, C. F. 1998, Combustion Flame, 114, 192
Pierre, M., et al. 1996, A&A, 315, L297
Piest, H., von Helden, G., & Meijer, G. 1999, ApJ, 520, L75
Puget, F., & Léger, A. 1989, ARA&A, 27, 161
Schutte, W. A., Tielens, A. G. G. M., & Allamandola, L. J. 1993, ApJ, 415, 397
Szczepanski, J., & Vala, M. 1993, ApJ, 414, 646
Verstraete, L., et al. 1996, A&A, 315, L337